JOURNAL OF THERMOPHYSICS AND HEAT TRANSFER
Vol. 10, No. 2, April–June 1996

Shape of an Evaporating Completely Wetting Extended Meniscus

Ihl Yong Kim*
Kolon Group Central Research Institute, Kyunggi-do 499-910, Republic of Korea
and
Peter C. Wayner Jr.†
Rensselaer Polytechnic Institute, Troy, New York 12180-3590

The microscopic details of fluid flow and heat transfer in the contact line region of an evaporating curved liquid film were experimentally and theoretically evaluated. The evaporating film thickness profiles were measured optically using null ellipsometry and image analyzing interferometry. These thickness profiles were analyzed using the augmented Young–Laplace equation to obtain the pressure field. Using the liquid pressure field, the evaporative mass flux profile was obtained from a Kelvin–Clapeyron model for the local vapor pressure. A correlation for the local slope (apparent contact angle) at a film thickness of $\delta = 20$ nm as a function of a dimensionless contact line heat sink was thereby obtained for a group of completely wetting fluids. This change in local slope leads to a decrease in the maximum value of the possible capillary suction at the base of the meniscus. A complementary macroscopic interfacial force balance was also used to describe the effects of viscous losses and interfacial forces on the local values of the apparent contact angle and curvature that are functions of the film thickness and heat flux. These two perspectives give a complete description of an evaporating, nonpolar, completely wetting curved film in the contact line region.

Nomenclature

A = $6\pi\bar{A}$, Hamaker constant
a, b = constants in Eq. (7), Eq. (8)
B = general form of dispersion constant
C = accommodation coefficient
K = interfacial curvature
k = thermal conductivity of the liquid film
L = length of control volume
M = molecular weight
$\dot{M}$ = dimensionless interfacial mass flux, Eq. (12)
$\dot{m}$ = evaporative mass flux
P = pressure
Q' = defined by Eq. (10)
q = heat flux
R = gas constant, radius of gap
T = temperature
x = coordinate distance along the substrate
Γ = mass flow rate per unit width
Δ = difference
Δh_m = heat of vaporization per unit mass
δ = thickness of the liquid film
δ_0 = reference interline film thickness
δ' = slope of the liquid–vapor interface
ε = defined by Eq. (3)
η = dimensionless film thickness, δ/δ_0
κ = dimensionless parameter, Eq. (13)
ν = kinematic viscosity
ξ = dimensionless distance
Π = disjoining pressure
Π_0 = characteristic pressure, Eq. (11)
σ = surface tension
$\bar{\tau}$ = average shear stress
ϕ = dimensionless pressure difference, Eq. (11)

Subscripts
c = over the regions $\delta_0 \leq \delta \leq 20$ or 40 nm
e = over the region $0 < \delta' \rightarrow \infty$
l = liquid
lv = liquid–vapor
s = solid
v = vapor
0 = at the interline

Superscript
id = ideal, defined by Eq. (12)

Received June 23, 1995; revision received Oct. 12, 1995; accepted for publication Oct. 17, 1995.

*Senior Researcher, Polymer Research and Development, Yongin-Gun.
†Professor of Chemical Engineering, Isermann Department of Chemical Engineering.

Introduction

THE microscopic details of fluid flow and heat transfer in the contact line region of an evaporating curved liquid film control the macroscopic performance of heat pipes and probably many other change-of-phase heat transfer processes (e.g., boiling). These transport processes depend on the temperature and intermolecular force fields. Herein, we discuss the results of an experimental and theoretical study of the microscopic transport processes occurring in the evaporating meniscus formed in the circular experimental cell presented in Fig. 1. The interline thickness δ_0 represents the junction of the evaporating and nonevaporating portions of the thin film. The region $\delta \leq \delta_0$ is kept from evaporating by the liquid–solid intermolecular adsorption forces that reduce the vapor pressure. The film thickness profile in the thickness range $\delta < 4$ μm was measured optically using null ellipsometry and image analyzing interferometry. Using the augmented Young–Laplace equation, the film thickness profile gives the pressure field in the evaporating thin liquid film. Using a Kelvin–Clapeyron (KC) model, the pressure and temperature fields give the evaporative heat flux profile. These analytical procedures also give the local slope (apparent contact angle) as a function

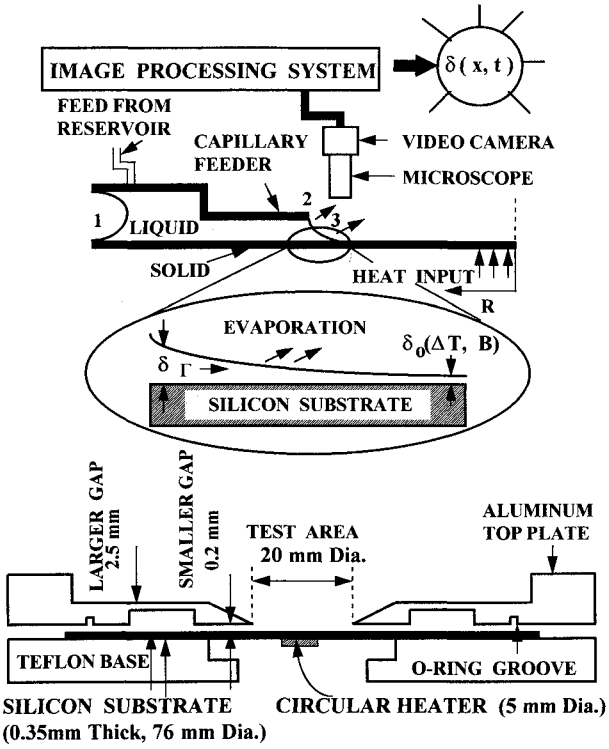

Fig. 1 Cross-sectional view of a circular capillary heat transfer cell. The gap thickness at location 2 is 2×10^{-4} m.

of the heat flow rate. The results demonstrate that there are significant resistances to heat transfer in a small meniscus due to interfacial forces, viscous stresses, and thermal conduction in the liquid. Therefore, the ideal heat sink based on kinetic theory and a constant curvature meniscus cannot be attained. To enhance this microscopic description of the transport processes, a complementary macroscopic interfacial force balance that relates the apparent contact angle to the interfacial forces and viscous losses is also developed and presented. These two perspectives give a complete description of an evaporating, nonpolar, completely wetting curved film in the contact line region.

Near liquid–vapor and liquid–solid interfaces, changes in the stress field occur within the liquid because of changes in the intermolecular force field. Interfacial free energies have been used to describe these changes. When the film thickness becomes extremely thin, additional changes occur because of the proximity of the two interfaces. The disjoining pressure concept has been used to describe these additional effects. For nonpolar systems the primary cause of the disjoining pressure is the van der Waals forces. In heat transfer, this description of the interfacial forces led to the development of the extended evaporating meniscus concept by Potash and Wayner,[1] which has been used to describe evaporative heat transfer in thin films (e.g., Refs. 2–7). Khrustalev and Faghri[8] and Swanson and Peterson[9,10] have used these models to analyze the microheat pipe. Recent use of the extended meniscus concept to describe portions of the microlayer in the related field of boiling[11–14] has also produced promising results. Previously, Pasamehmetoglu et al.[14] demonstrated that dominant evaporation at the contact line is required to match the boiling curve quantitatively. Therefore, we anticipate that these concepts will be of general use in change-of-phase heat transfer.

Herein, we obtain additional insights concerning the evaporating meniscus by analyzing new data and by obtaining a correlation for the local slope (apparent contact angle) at a particular film thickness (δ = 20 nm) as a function of a dimensionless contact line heat sink for a group of completely wetting fluids. In addition, we present and use a macroscopic force balance for some of the new data to complete the description of the effect of transport processes in the contact line region.

Macroscopic Interfacial Force Balance

For a complete description of the evaporating meniscus, we use both the macroscopic (integral) and microscopic (differential) viewpoints. A macroscopic horizontal force balance for the completely wetting ($\bar{A} < 0$), nonpolar, meniscus presented in Fig. 2 gives

$$\sigma_{lv} \cos\theta + \sigma_{ls} + \sigma_{lv} K\delta + (-\bar{A}/\delta^2) + \bar{\tau}L = \sigma_{lv0} + \sigma_{ls0} + \sigma_{lv0} K_0 \delta_0 + (-\bar{A}/\delta_0^2) \quad (1)$$

$\bar{\tau}$ is the average shear stress over the length L. Background for the interfacial forces that led to this result can be found in literature.[15–17] Equation (1) can be simplified using the following assumptions: $\sigma_{ls} = \sigma_{ls0}$, $\sigma_{lv} = \sigma_{lv0}$, $K_0 = 0$, in which the subscript 0 refers to the location of the interline δ_0. The first two assumptions restrict the contact line thickness to approximately $\delta_0 > 1$ nm and the third assumes that the substrate is smooth. The resulting Eq. (2) applies to the experimental conditions discussed as follows:

$$\sigma_{lv}(1 - \cos\theta) = \bar{\tau}L + \sigma_{lv} K\delta + (\bar{A}/\delta_0^2) - (\bar{A}/\delta^2) \quad (2)$$

We find that the apparent contact angle θ at the thicker end is a function of the downstream viscous losses and interfacial forces. The curvature at this location can approach a constant asymptotic value if the thickness δ is sufficiently large so that the upstream viscous stresses are relatively minor. Previously, Wayner[18] used this change in apparent contact angle in the contact line region to define a percent decrease in fluid flow (relative to that in a constant curvature meniscus) to the base of an evaporating meniscus in a capillary as

$$\varepsilon = 100(1 - \cos\theta) \quad (3)$$

The symbol ε is a measure of the decrease in the available capillary suction at the base of the meniscus.

Microscopic Theory and Experiments

Only a very brief description of the experiments using the circular capillary feeder system presented in Fig. 1 is given herein. The experimental details are given elsewhere by DasGupta et al.[5,19] and Kim.[20] The experimental substrate was a single crystal silicon with a native oxide of about 3 nm. Liquid flowed from a reservoir as a result of a difference in capillary and disjoining pressure (caused by intermolecular forces) and formed an extended meniscus at the edge of the

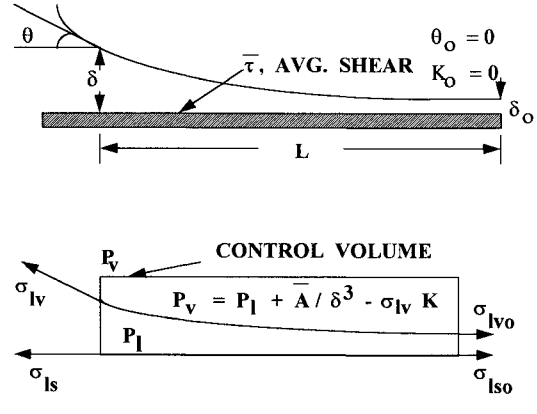

Fig. 2 Control volume for macroscopic horizontal force balance due to interfacial free energy with $\bar{A} < 0$.

thinner gap at position 3. The temperature in the contact line region, area 3, governed the critical initial film thickness condition δ_0 for the behavior of the evaporating meniscus. Because of adsorption, evaporation did not occur in the thinnest portion of the meniscus represented by $\delta = \delta_0$. The details of the liquid film thickness profile in the contact line region were measured as a function of the evaporation rate using ellipsometry for δ_0 and microcomputer enhanced video microscopy based on interferometry for $\delta > \delta_0$.

The development of the model, boundary conditions, and the numerical solution scheme have been discussed in great detail.[5,19,20] We will only introduce the basic model equations because the main objective of this article is to give an expanded view of the resulting description of the physical phenomena. The liquid pressure P_l is related to the vapor phase pressure P_v by the following augmented Young–Laplace equation, which accounts for both the disjoining and capillary pressures in the liquid film:

$$P_l - P_v = \frac{\bar{A}}{\delta^3} - \sigma \frac{d^2\delta}{dx^2} \tag{4}$$

The first term on the right-hand side of Eq. (4) is called the disjoining pressure Π, and it is an effective pressure that represents the van der Waals body force on the liquid due to dispersion phenomena. Using a lubrication model, the mass flow rate per unit width of the film $\Gamma(x)$ in a slightly tapered thin film is

$$\Gamma(x) = \frac{-1}{3v} \delta^3 \frac{d}{dx} [P_l] \tag{5}$$

Equations (4) and (5) demonstrate that the mass flow rate is a function of the thin film shape $\delta(x)$. The evaporative flux is linked to the flow rate in the film through a material balance:

$$\dot{m} = -\frac{d\Gamma}{dx} \tag{6}$$

Wayner et al.[2,17,21] developed a KC model for the evaporative flux as a function of the temperature and pressure jumps at the interface according to the expression:

$$\dot{m} = a(T_{lv} - T_v) + b(P_l - P_v) \tag{7}$$

$$a = C \left(\frac{M}{2\pi R T_{lv}}\right)^{1/2} \left(\frac{P_v M \Delta h_m}{R T_v T_{lv}}\right)$$
$$b = C \left(\frac{M}{2\pi R T_{lv}}\right)^{1/2} \left(\frac{V_l P_v}{R T_{lv}}\right) \tag{8}$$

According to Eq. (7) evaporation is promoted by superheat and hindered by low liquid film pressure. Following Moosman and Homsy,[22] the one-dimensional heat conduction heat transfer solution for the film is used to eliminate T_{lv} in favor of T_s in Eq. (7), giving Eq. (9):

$$\dot{m} = \frac{1}{1 + (a\Delta h_m/k)\delta} [a(T_s - T_v) + b(P_l - P_v)] \tag{9}$$

This equation clearly demonstrates the direct effect of film thickness and intermolecular forces on the evaporation rate. This model implies that the vapor and solid phases do not present significant resistances to evaporation. We note that in our experiments the thermal conductivity of silicon is very large. We also note that, for additional insight, Stephan and Busse[6] have numerically evaluated the details of the effect of substrate thermal conductivity on the evaporating meniscus.

The nondimensionalized form of the governing equations were solved numerically and compared with the experimental data on the film profile and substrate temperature to obtain the results presented next.[15,19] Consistent and justifiable results were obtained that we believe confirm the validity of the KC model. We note that a successful heat balance was obtained by Kim,[20] which can be used as a measure of the overall accuracy of the results. For one of the runs the measured mass flow rate from the capillary feeder was found to be 26% higher than the evaporative mass flow rate from the meniscus based on the KC model. Considering the number of experimental and modeling procedures associated with this type of microscopic study, this represents good agreement. The errors in the measurement techniques were discussed by DasGupta et al.[5] The final estimate was an error of about 0.4 nm for the adsorbed thin film region measured by ellipsometry. The maximum error in the capillary meniscus region was less than 0.01 μm, based on repeated measurements and the maximum value of the error decreased (always within 5%) as the thin film was approached.

Experimental Results and Discussion

The experimental thickness profiles were evaluated and compared with a model equation using the procedures outlined by DasGupta et al.[5,19] The measured values of $\delta^{1/2}$ vs the relative distance x for octane are given in Fig. 3 as a function of the total evaporative heat flow rates per unit width of the meniscus Q_e':

$$Q_e' = \int_0^{L_e} q \, dx \tag{10}$$

where L_e represents the length of the region where $0 < \delta' \rightarrow \infty$. The procedures for obtaining the value of this integral are given by Kim.[20] These results demonstrate that the thickness of the adsorbed film δ_0 decreased with an increase in Q_e', which increases with the substrate temperature. In an isothermal horizontal system of a spreading liquid on a solid substrate at the exit of a capillary, the curvature should remain constant in the region where dispersion forces can be neglected, so that the film profile in this range approximates a parabola and a plot of $\delta^{1/2}$ vs x is a straight line. For the case where $Q_e' \rightarrow 0$ W/m, $\delta^{1/2}$ vs x is nearly a straight line, which means the system was very close to isothermality. However, for the cases involving evaporation, the lines bend downward, thereby show-

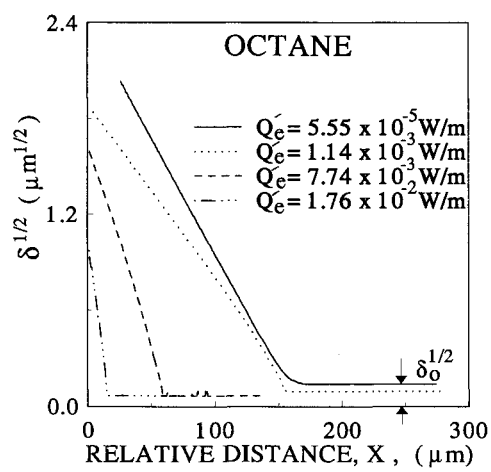

Fig. 3 Experimental values of $\delta^{1/2}$ vs the relative distance x for octane for various heat flow rate per unit width: Q_e' = 5.55 × 10^{-5} W/m, δ_0 = 1.9 × 10^{-8} m, Π_0 = 1.09 × 10^1 N/m^2; Q_e' = 1.14 × 10^{-3} W/m, δ_0 8.9 × 10^{-9} m, Π_0 = 4.11 × 10^1 N/m^2; Q_e' = 7.74 × 10^{-3} W/m, δ_0 = 4.5 × 10^{-9} m, Π_0 = 3.20 × 10^2 N/m^2; and Q_e' = 1.76 × 10^{-2} W/m, δ_0 = 4.4 × 10^{-9} m, Π_0 = 8.86 × 10^2 N/m^2.

ing the presence of a curvature gradient that causes fluid flow. These results clearly demonstrate that the film thickness profile and curvature are definitely functions of the heat flux. The evaporative flux is connected to the viscous losses by Eqs. (5) and (6). The suction at δ_0 is equal to Π_0 and is a function of the substrate superheat.

In Fig. 4 an example of the dimensionless pressure ϕ and curvature, obtained from fitting the data with the KC model, is presented as a function of the dimensionless film thickness η for octane in which

$$\eta = \delta/\delta_0, \qquad \Pi_0 = -(\bar{A}/\delta_0^3), \qquad \phi = (P_l - P_v)/\Pi_0 \quad (11)$$

The dimensional interfacial pressure difference can be obtained by multiplying ϕ by the reference disjoining pressure Π_0. We find that, for a completely wetting system, the curvature starts at zero and becomes a maximum due to a change in the disjoining pressure and then decreases when it becomes the dominant cause of fluid flow. We also find that, in the thicker region, the curvature approaches a constant value because of the decrease in viscous losses.

The dimensionless interfacial flux $\dot{M}$ is related to ϕ by

$$\dot{M} = \frac{\dot{m}}{\dot{m}^{id}} = \frac{q}{q^{id}} = \frac{1+\phi}{1+\kappa\eta}$$
$$\dot{m}^{id} = C\left(\frac{M}{2\pi RT_{lv}}\right)^{1/2}\left(\frac{P_v M \Delta h_m}{RT_v T_{lv}}\right)(T_{lv} - T_v) \quad (12)$$

in which

$$\kappa = a\Delta h_m \delta_0 / k \quad (13)$$

The parameter κ is a measure of the importance of the resistance of the film to thermal conduction. In Fig. 5 the dimensionless interfacial evaporative flux profiles are presented for various heat flow rates per unit width of the meniscus. In the adsorbed thin film region, where the film thickness is δ_0, the dimensionless pressure is $\phi = -1$. Therefore, the dimensionless interfacial flux is equal to zero. This result is due to the London van der Waals force, which keeps the superheated thin film from evaporating. The absolute value of ϕ decreases as the thickness increases. Therefore, the interfacial evaporative flux increases due to the decrease in the effect of interfacial forces. This increase is partially offset by the decline of the interfacial flux resulting from the rise of the conductive resistance that is due to the increase in the film thickness. Therefore, a maximum is obtained in the flux profile. Additional details concerning the numerical values of the conductive resistances can be found in DasGupta et al.[23]

The apparent contact angle of the meniscus at the film thickness δ is

$$\theta|_\delta = \tan^{-1}\left(\frac{d\delta}{dx}\right)_\delta \quad (14)$$

In Fig. 6 the slope of the meniscus at $\delta = 40$ nm is presented as a function of the value of the evaporative heat flow rate per unit width of the meniscus in the region $\delta_0 \leq \delta \leq 40$ nm, Q_c'. We note that Q_c' represents a much smaller region than Q_e'. These results clearly demonstrate that the slope at a particular thickness is a function of the evaporation rate. In Fig. 7 the slope of the meniscus at $\delta = 20$ nm is presented as a function of a dimensionless contact line heat sink. Using this data, a simple correlation for the slope at $\delta = 20$ nm can be obtained

$$\delta' = 0.021\left(\frac{-Q_c'\delta\nu}{\bar{A}\Delta h_m}\right)^{0.69}, \qquad \bar{A} < 0, \qquad \delta = 20 \text{ nm} \quad (15)$$

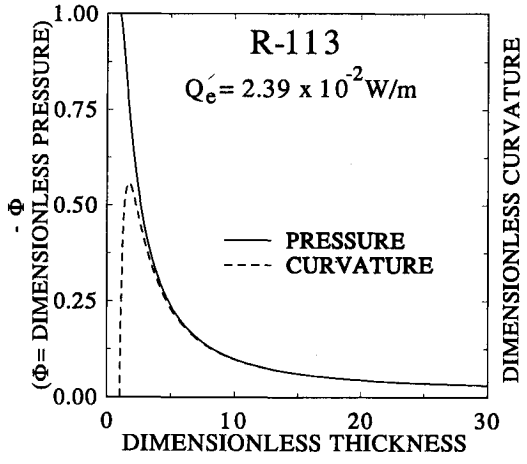

Fig. 4 Dimensionless pressure and curvature profiles, $\delta_0 = 3.9$ nm, $\Pi_0 = 2.2 \times 10^3$ N/m^2, $Q_e' = 2.39 \times 10^{-2}$ W/m.

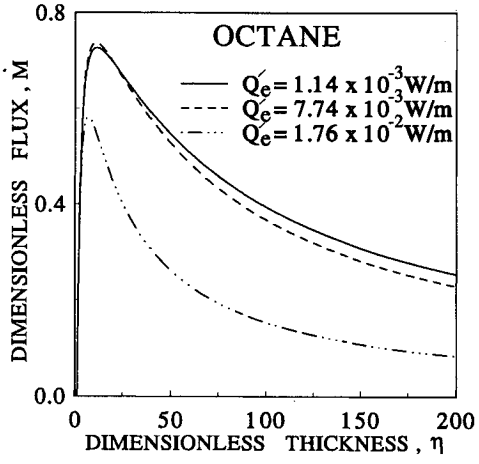

Fig. 5 Dimensionless flux vs dimensionless thickness: $Q_e' = 1.14 \times 10^{-3}$ W/m, $\delta_0 = 8.9 \times 10^{-9}$ m, $m^{id} = 2.76 \times 10^{-5}$ kg/m^{2}s, $q^{id} = 10$ W/m^2; $Q_e' = 7.74 \times 10^{-3}$ W/m, $\delta_0 = 4.5 \times 10^{-9}$ m, $m^{id} = 6.42 \times 10^{-4}$ kg/m^{2}s, $q^{id} = 223$ W/m^2; $Q_e' = 1.76 \times 10^{-2}$ W/m, $\delta_0 = 4.4 \times 10^{-9}$ m, $m^{id} = 7.42 \times 10^{-3}$ kg/m^{2}s, $q^{id} = 2329$ W/m^2.

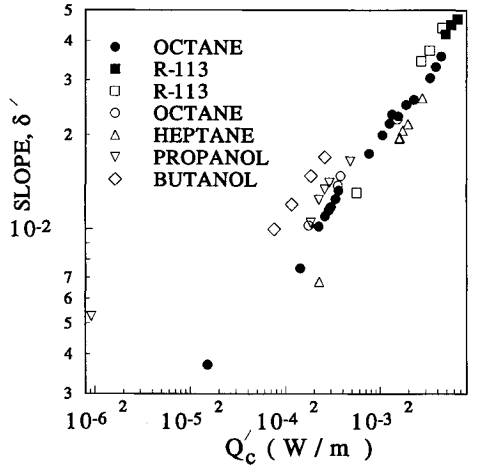

Fig. 6 Interfacial slope at $\delta = 40$ nm vs Q_c'.

where Q_c' is the value of the evaporative heat flow rate per unit width of the meniscus in the region $\delta_0 \leq \delta \leq 20$ nm. The background for this dimensionless number is given by Wayner.[24] This dimensionless group gives the effect of the system properties (ν, Δh_m, $\bar{A}$) on the heat flow rate. An increase in viscous effects (ν and flowrate associated with Q_c') gives a

larger slope, whereas a higher heat of vaporization reduces the need for fluid flow. We note that, since this number was theoretically developed for a much thinner film thickness, it can only be used to correlate the data at this thickness. In Fig. 8, the local slope obtained from the KC model is presented as a function of film thickness for octane at various values of Q_e'. These results demonstrate that the slope starts from zero in the equilibrium thin film region ($\delta = \delta_0$), increases rapidly, and then becomes a weaker function of film thickness or distance

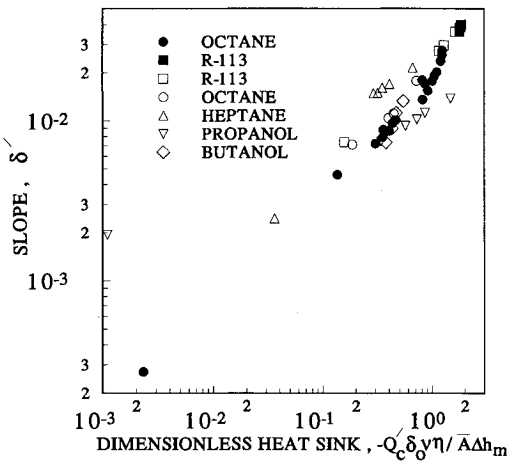

Fig. 7 Slope vs dimensionless heat sink, $-Q_e'\delta_0\nu\eta/\bar{A}\Delta h_m$, at a film thickness δ = 200 Å.

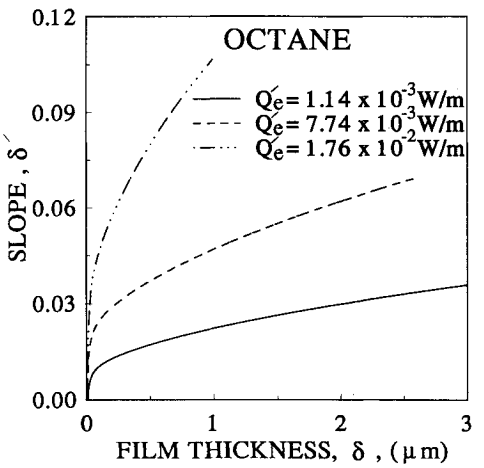

Fig. 8 Slope vs film thickness for octane for various heat flow rates per unit width Q_e'.

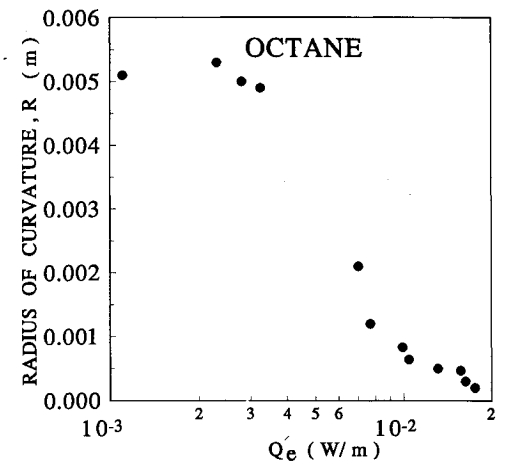

Fig. 9 Radius of curvature at δ = 1 μm vs Q_e'.

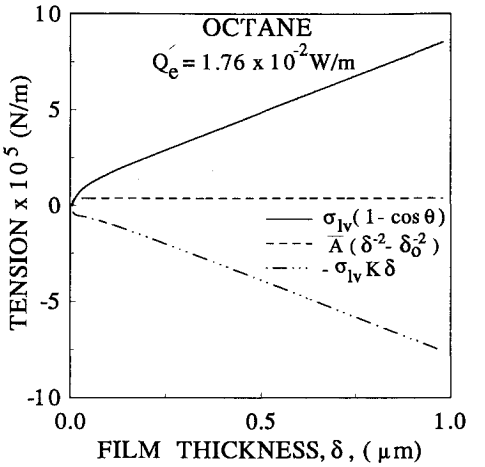

Fig. 10 Comparison of terms in Eq. (2).

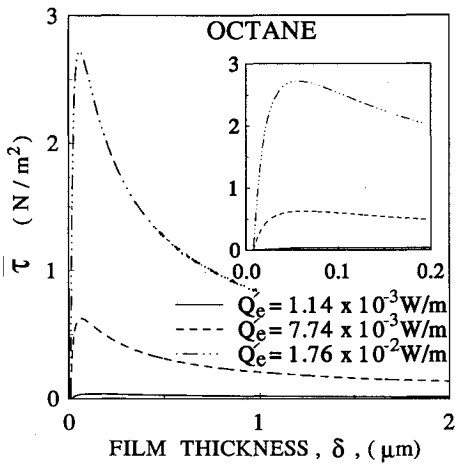

Fig. 11 Average shear stress in the region $\delta > \delta_0$ vs δ.

in the thicker film region. We find that, due to viscous losses, the slope and the magnitude of the apparent contact angle θ increases with an increase in the heat flow rate per unit width of the meniscus Q_e'. These results also indicate that for large rates of heat transfer there would be a significant decrease in the maximum attainable capillary suction at the base of the meniscus due to viscous losses in the evaporating meniscus [Eq. (3)]. It is important to note that there are two possible viscous effects on the curvature at the base of the meniscus: 1) one upstream of the meniscus base in the supply line and 2) one downstream of the meniscus base in the curved evaporating film. We tried to keep the overall upstream total head change constant by adjusting the reservoir height. Therefore, the profile changes we report are due to viscous losses in the meniscus. Using the model that agreed with the data, these effects are described in the previous figures. Since the size of the meniscus decreases with heat flux, the local radius of curvature also decreases with an increase in the evaporative heat flow rate per unit width of the meniscus. This is demonstrated in Fig. 9 in which the radius of curvature at δ = 1 μm is presented as a function of Q_e'. This thickness is outside the region presented in Fig. 4. Twice the minimum radius of curvature in Fig. 9 is larger than the smaller gap width in Fig. 1.

The previous description of the evaporating meniscus is enhanced by the following details associated with the macroscopic model. In Figs. 10 and 11, the values of the various terms in Eq. (2) are compared. The change in $\sigma_{lv}(1 - \cos\theta)$ vs film thickness is presented in Fig. 12 for various values of Q_e'. As described by Eqs. (2) and (3), the viscous losses in this very thin film region have a significant effect on the curvature at the base of the meniscus. For a constant curvature region,

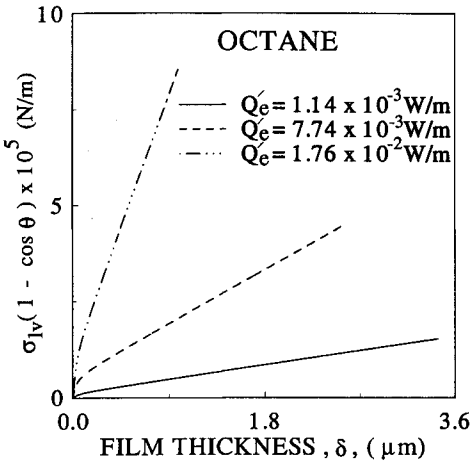

Fig. 12 Change in $\sigma_{lv}(1 - \cos \theta)$ vs film thickness.

$\sigma_{lv}(1 - \cos \theta)$ is a linear function of thickness. Therefore, we find that there is a very small but very important region near the interline where the curvature changes rapidly. The viscous losses in the part of the evaporating meniscus have the dominant effect on the base curvature. Upstream from this region the curvature gradient is relatively small.

Conclusions

1) The augmented Young–Laplace and the Kelvin–Clapeyron differential models of the effect of interfacial forces on the characteristics of an evaporating meniscus describe the microscopic details of heat and mass transfer.

2) The macroscopic interfacial force model gives a complementary integral view of the evaporating meniscus.

3) The shape (thickness, slope, curvature, and apparent contact angle) of the liquid–vapor interface is a function of the evaporative heat flow rate per unit width of the meniscus, which leads to a reduction in the maximum value of the possible suction potential at the base of an evaporating meniscus.

4) The viscous losses that are directly related to the flow of the evaporating liquid in the thinnest part of the evaporating meniscus have the dominant effect on the base curvature (if supply side losses are neglected).

Acknowledgments

This material is based on work supported by the National Science Foundation under Grant CTS-9123006. The initial data presented in Figs. 3, 5, 7, and 8 were published in the Proceedings of the IX International Heat Pipe Conference, Albuquerque, New Mexico, May 1–5, 1995.

References

[1]Potash, M., Jr., and Wayner, P. C., Jr., "Evaporation from a Two-Dimensional Extended Meniscus," *International Journal of Heat and Mass Transfer*, Vol. 15, No. 10, 1972, pp. 1851–1863.

[2]Wayner, P. C., Jr., Kao, Y. K., and LaCroix, L. V., "The Interline Heat Transfer Coefficient of an Evaporating Wetting Film," *International Journal of Heat and Mass Transfer*, Vol. 19, No. 5, 1976, pp. 487–492.

[3]Kamotani, Y., "Evaporator Film Coefficients of Grooved Heat Pipes," *A Collection of Technical Papers of the 3rd International Heat Pipe Conference* (Palo Alto, CA), AIAA, New York, 1978, pp. 128, 129.

[4]Holm, F. W., and Goplen, S. P., "Heat Transfer in the Meniscus Thin-Film Transition Region," *Journal of Heat Transfer*, Vol. 101, No. 3, 1979, pp. 543–547.

[5]DasGupta, S., Schonberg, J. A., Kim., I. Y., and Wayner, P. C., Jr., "Use of the Augmented Young–Laplace Equation to Model Equilibrium and Evaporating Extended Menisci," *Journal of Colloid and Interface Science*, Vol. 157, No. 2, 1993, pp. 332–342.

[6]Stephan, P. C., and Busse, C. A., "Analysis of the Heat Transfer Coefficient of Grooved Heat Pipe Evaporator Walls," *International Journal of Heat and Mass Transfer*, Vol. 35, No. 2, 1992, pp. 383–391.

[7]Hallinan, K. P., Cherbaro, H. C., Kim, S. J., and Chang, W. S., "Evaporation from an Extended Meniscus for Nonisothermal Interfacial Conditions," *Journal of Thermophysics and Heat Transfer*, Vol. 8, No. 4, 1994, pp. 709–716.

[8]Khrustalev, D., and Faghri, A., "Thermal Analysis of a Micro Heat Pipe," *Journal of Heat Transfer*, Vol. 116, No. 1, 1994, pp. 189–198.

[9]Swanson, L. W., and Peterson, G. P., "The Interfacial Thermodynamics of the Capillary Structures in Micro Heat Pipes," *Heat Transfer on the Microscale*, HTD-Vol. 253, American Society of Mechanical Engineers, New York, 1993, pp. 45–51.

[10]Swanson, L. W., and Peterson, G. P., "Evaporating Extended Meniscus in a V-Shaped Channel," *Journal of Thermophysics and Heat Transfer*, Vol. 8, No. 1, 1994, pp. 172–180.

[11]Wayner, P. C., Jr., "Thermal and Mechanical Effects in the Spreading of a Liquid Film Due to a Change in the Apparent Finite Contact Angle," *Journal of Heat Transfer*, Vol. 116, No. 4, 1994, pp. 938–944.

[12]Lay, J. H., and Dhir, V. K., "A Nearly Theoretical Model for Fully Developed Nucleate Boiling of Saturated Liquids," *Heat Transfer 1994, Proceedings of the 10th International Heat Transfer Conference, Brighton, England, UK*, Vol. 5, Inst. of Chemical Engineers, Rugby, Warwickshire, England, UK, 1994, pp. 105–110.

[13]Stephan, P. C., and Hammer, J., "A New Model for Nucleate Boiling Heat Transfer," *Warme- und Stoffubertragung*, Vol. 30, No. 2, 1994, pp. 119–125.

[14]Pasamehmetoglu, K. O., Chappidi, P. R., Unal, C., and Nelson, R. A., "Saturated Pool Nucleate Boiling Mechanisms at High Heat Fluxes," *International Journal of Heat and Mass Transfer*, Vol. 36, No. 15, 1993, pp. 3859–3868.

[15]deFeijter, J. A., "Thermodynamics of Thin Liquid Films," *Thin Liquid Films, Fundamentals and Applications*, edited by I. B. Ivanov, 1st ed., Marcel Dekker, New York, 1988, pp. 1–47.

[16]Martynov, G. A., Starov, V. M., and Churaev, N. V., "Hysteresis of the Contact Angle at Homogeneous Surfaces," *Kolloidnyi Zhurnal* (English Translation), Vol. 39, No. 3, 1977, pp. 406–417.

[17]Wayner, P. C., Jr., "The Effect of Interfacial Mass Transport on Flow in Thin Liquid Films," *Colloids and Surfaces*, Vol. 52, No. 1, 1991, pp. 71–84.

[18]Wayner, P. C., Jr., "Effect of Thin Film Heat Transfer on Meniscus Profile and Capillary Pressure," *AIAA Journal*, Vol. 17, No. 7, 1979, pp. 772–776.

[19]DasGupta, S., Schonberg, J. A., and Wayner, P. C., Jr., "Investigation of an Evaporating Extended Meniscus Based on the Augmented Young-Laplace Equation," *Journal of Heat Transfer*, Vol. 115, No. 1, 1993, pp. 201–208.

[20]Kim, I. Y., "An Optical Study of the Heat Transfer Characteristics of an Evaporating Thin Liquid Film," Ph.D. Dissertation, Rensselaer Polytechnic Inst., Troy, New York, 1994.

[21]Wayner, P. C., Jr., DasGupta, S., and Schonberg, J. A., "Effect of Interfacial Forces on Evaporative Heat Transfer in a Meniscus," WL-TR-91-2061, Wright–Patterson AFB, Ohio, Sept. 1991.

[22]Moosman, S., and Homsy, S. M., "Evaporating Menisci of Wetting Fluids," *Journal of Colloid and Interface Science*, Vol. 73, No. 1, 1980, pp. 212–223.

[23]DasGupta, S., Kim., I. Y., and Wayner, P. C., Jr., "Use of the Kelvin-Clapeyron Equation to Model an Evaporating Curved Microfilm," *Journal of Heat Transfer*, Vol. 116, No. 4, 1994, pp. 1007-1015.

[24]Wayner, P. C., Jr., "A Dimensionless Number for the Contact Line Evaporative Heat Sink," *Journal of Heat Transfer*, Vol. 111, No. 3, 1989, pp. 813–815.